Algorithm for automatic detection and analysis of cracks in timber beams from LiDAR data

Cabaleiro, M.; Lindenbergh, R.; Gard, W. F.; Arias, P.; van de Kuilen, J. W G

DOI
10.1016/j.conbuildmat.2016.11.032

Publication date
2017

Document Version
Accepted author manuscript

Published in
Construction and Building Materials

Citation (APA)
Cabaleiro, M., Lindenbergh, R., Gard, W. F., Arias, P., & van de Kuilen, J. W. G. (2017). Algorithm for automatic detection and analysis of cracks in timber beams from LiDAR data. *Construction and Building Materials*, *130*, 41-53. https://doi.org/10.1016/j.conbuildmat.2016.11.032

Postprint of Construction and Building Materials
Volume 130, 15 January 2017, Pages 41–53
Link to formal publication (Elsevier): http://dx.doi.org/110.1016/j.conbuildmat.2016.11.032

Algorithm for automatic detection and analysis of cracks in timber beams from LiDAR data

M.Cabaleiro[1]*, R. Lindenbergh[2], W.F. Gard[3], P. Arias[4], J.W.G. van de Kuilen[5].

[1] Department of Materials Engineering, Applied Mechanics and Construction, School of Industrial Engineering, University of Vigo, 36208, Vigo, Spain.

[2] Department of Geoscience and Remote Sensing, Delft University of Technology, Stevinweg 1, 2628 CN Delft, The Netherlands.

[3] Department of Structural Engineering, Section: Timber Structure and Wood Technology, Delft University of Technology, Stevinweg 1, 2628 CN Delft, The Netherlands.

[4] Department of Natural Resources and Environmental Engineering, School of Mining Engineering, University of Vigo, 36310, Vigo, Spain.

[5] Wood Research Institute, Technical University of Munich, Winzererstrasse 45, 80797, Munich, Germany

*Corresponding author: mcabaleiro@uvigo.es; tel: +34 986 813659. Fax: +34 986 813663

Abstract: Cracks may indicate structural problems in constructions made of timber beams, but their identification in notably roof constructions is difficult. Therefore this paper presents an algorithm for the automatic detection of cracks in timber beams sampled by LiDAR data. This algorithm enables the identification, analysis and monitoring of cracks and their geometrical characteristics. The algorithm is validated by tests on laboratory specimens and on a timber roof structure. The results prove that the proposed algorithm is able to automatically identify and analyze cracks with a width of above 3 mm from point clouds with an average resolution below 1 mm.

Key words: Wood, crack, alpha-shapes, laser scanning.

1. Introduction

Along history, wood has been a material commonly used in the construction of all kind of buildings and structures, such as houses, bridges, towers, windmills, etc. In fact, nowadays there are innumerable historical timber structures around the world. To preserve this heritage, its conservation and maintenance is needed. For this reason, structural health control is a fundamental issue. Also for the rehabilitation of old buildings for alternative use, analysis of structural health is mandatory. During the last century the use of wood as material for structures has declined in favor of other materials such as steel or concrete. Nevertheless, in recent decades the use of both solid and engineered laminated timber in structures has increased again.

1.1 Cracks in timber

Natural wood generally cracks when it dries. This is caused by the anisotropic behavior of wood in radial versus tangential direction along the cross-section of the beam (Figure 1a). Cracks are present in both old and new structures. For new timber structures mainly glue laminated timber is used. Cracks may develop within the timber lamella or in the glue line and this is generally caused by stresses perpendicular to the grain as a result of temperature and wood moisture fluctuations in the beam (Figure 1b). The loading and the duration or variation of loading also influence crack growth, especially in areas with complex stress states.

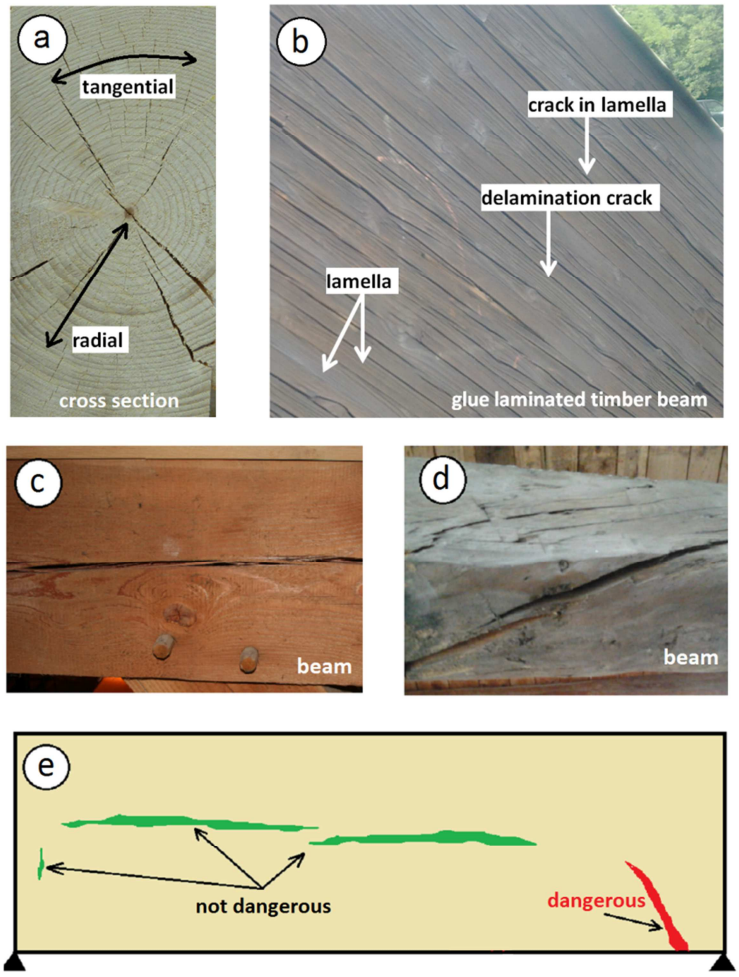

Figure 1. (a) Cross section of a timber beam with cracks in radial direction. (b) Glue laminated timber beam (side view) with cracks in the lamella and in the glue line (delamination cracks). (c) Example of an almost straight and continuous drying crack (d) Example of a serious crack crossing almost the entire- cross section. (c) Sketch of not dangerous and dangerous cracks, the green cracks generally are less dangerous than the red one, but it depends on the beam loading and remaining functional cross section.

Many cracks are harmless, but other cracks negatively affect the strength of a structure. Depending on the position, size and shape of the crack, it may have consequences for the safety of the structure, which in addition depends on the beam loading (Figure 1e). For example, large cracks in the neutral axis of a beam decrease the load bearing capacity of the timber element in shear and can also result

in a new stress distribution which may result in crack propagation. Cracks following the grain (fibre) that deviate from the neutral axis need to be evaluated depending on their size and location (Figure 1d). Mapping beam cracks is a necessary task to evaluate their potential danger. The potential impact of a crack could be determined after crack detection using finite element analysis. Mapping all cracks in for example a wooden roof structure using contact measurements is time consuming and often challenging, because of the height of the structure above the floor. The importance of the depth of a crack for solid wood strength properties has been investigated by Frech [1]. High growth rates, the presence of pits, knots and juvenile wood in the beam increases the hazard of developing cracks [2]. However for service life prediction and safety considerations, controlling and evaluation of arising and growing cracks are essential.

1.2 Methods and techniques for crack analysis

For initial inspection and control of building and structures, non-destructive methods are most suitable because the material is not, or very limited, damaged by the measurements. Examples of such methods are: acoustic methods, resistance drilling techniques and radiography [3-5]. Also some inspection work has been performed using Ground Penetrating Radar (GPR) [6]. These methods allow a detailed analysis of the health of a timber structure but, they have the disadvantage that it is necessary to access the object and make contact with it.

Photogrammetry is a technique which enables health monitoring without direct contact of the scene. Several researchers have applied photogrammetry to assess cracks. Barazzetti and Scaioni [7] present an image-based method for crack analysis; Sohn et al. [8] propose a crack-monitoring system to quantify the change of cracks in concrete from multitemporal images. Patricio and Maravall [9] present a novel generalization of the gray-scale histogram and its application to the automated visual measurement and inspection of cracks in wooden pallets. Although photogrammetry is in general a suitable technique to assess cracks, photogrammetry also depends on the light, color and texture of

the specimen surface to analyze. In some indoor situations bad lighting conditions may therefore hamper the use of photogrammetry for crack analysis.

Laser scanning is a promising alternative technique for tstructural health analysis [10-12]. Laser scanning provides several advantages with respect to other methods such as: enabling the analysis of inaccessible structural elements, obtaining the 3D surface without direct contact to the specimen, efficient data collection in the form of ready to use 3D point clouds, no dependency on lighting conditions, color and texture of the specimen surface under analysis. Some applications of laser scanning for structural analysis are: dimensional compliance control [13] , construction progress control [14] , analysis and documentation of historic structures [15,16], 3D modeling for structural engineering purposes [17-19] or analysis of structural health [11-12].

In the field of timber structures, laser scanning has been successfully used for 3D modeling of historic structures. Alessandri and Mallardo [20] deals with some preliminary structural analysis of the wooden roof construction of the Church of the Nativity in Bethlehem; Balletti et al. [21] study the wooden roof structure of the dome of SS. Giovanni e Paolo in Venice; Oreni et al. [22] illustrates the switch from a 3D content model to a Historic Building Information Model (HBIM) in order to support conservation and management of built heritage. However, to the best of our knowledge only Van Goethem et al [23] has reconstructed and modeled timber boards with knots from LiDAR data. Knots and their location in the boards were analysed and structural wood quality could be estimated.

Some work has been performed on the analysis of cracks sampled by LIDAR data in non-wooden structures. Laefer et al. [24] presents the fundamental mathematics to determine the minimum crack width detectable with a terrestrial laser scanner in unit-based masonry; Laefer et al. [25] compares the relative performance capabilities of crack detection by sidewalk-based manual inspection with digital photography. Sánchez-Aparicio et al. [26] presents a set of procedures based on laser scanning, photogrammetry and operational modal analysis to improve calibration of finite element

models in historical buildings. This work includes cracks in masonry walls. In the same way, Huang et al. [26] present a pavement crack detection method combining 2D and 3D information based on Dempster-Shafer Theory. Nevertheless, none of these works address the automatic detection and quantification of cracks in wood structures from LIDAR data.

The aim of this paper is to develop a first algorithm for the automatic detection of cracks in timber beams from LiDAR data. This algorithm allows analyzing the geometric characteristics of each identified crack, as well as generating a data file that labels each crack including all of its geometric characteristics. This algorithm will in addition be used for monitoring the possible growth of each crack in time. After this introduction, Section 2 outlines the proposed and developed algorithm. In Section 3 a series of tests with laboratory specimens and real timber structures are performed to check the algorithm and experimental results are presented. In Section 4 results and applicability of the proposed method are discussed. Finally, in Section 5, conclusions are given.

2. Methodology

The general methodology used in this paper for the automatic detection of cracks and controlling crack growth between different epochs is shown in Figure 2.

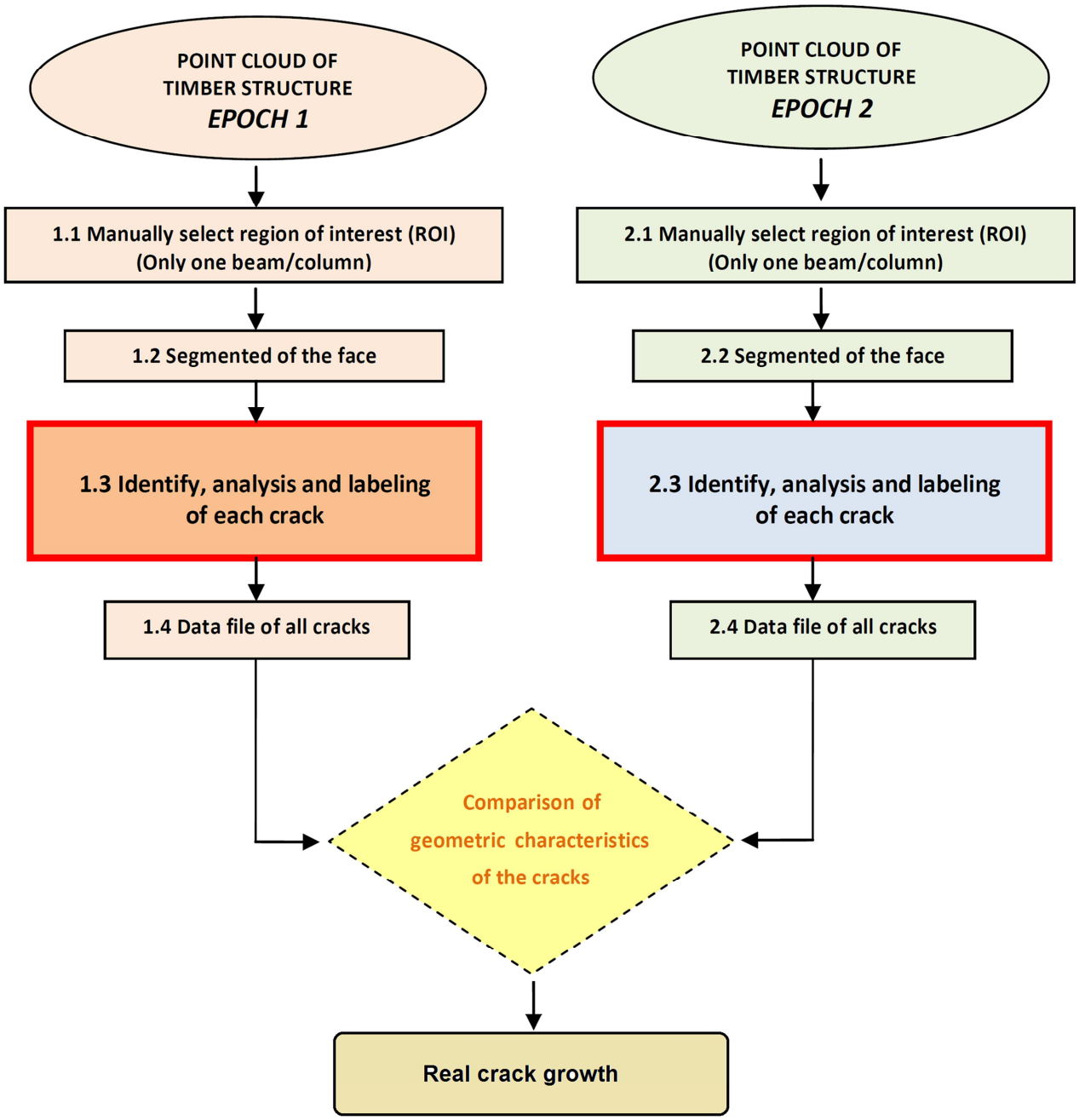

Figure 2. Workflow of the general methodology used in this paper.

The process begins with the scanning of the timber structure. Within the point clouds obtained by the laser scanner, a region of interest (ROI) that contains the beam to analyze is selected. This is the only manual step in the whole process, which is performed with commercial software for point cloud processing. Next, the segmentation of the face of the beam to analyze is performed. For this segmentation a RANSAC algorithm [27-28] is used. From this segmented face, the new algorithm

proposed in this work is used to identify, analyze and label each crack. As a result, a data file with all geometric characteristics of each identified crack is obtained. This file will be used in future for controlling the crack growth during different periods of time, by comparing the geometric characteristics of the cracks between the initial Epoch 1 and some consecutive Epoch 2. Figure 3 summarizes the workflow of the novel algorithm that is proposed to find and analyze cracks.

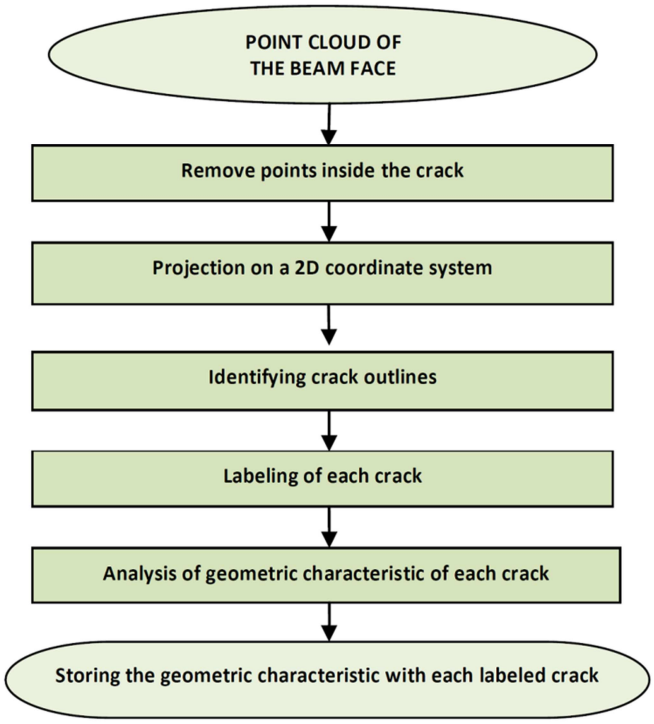

Figure 3. Workflow of the novel methodology to find cracks.

Next, the steps of the proposed novel algorithm are described in detail below.

2.1. Removing points inside the crack

During the segmentation of the timber beam face, points that belong to the inside of the crack may remain (Figure 4). These points must be deleted to prevent errors at the next steps of the algorithm.

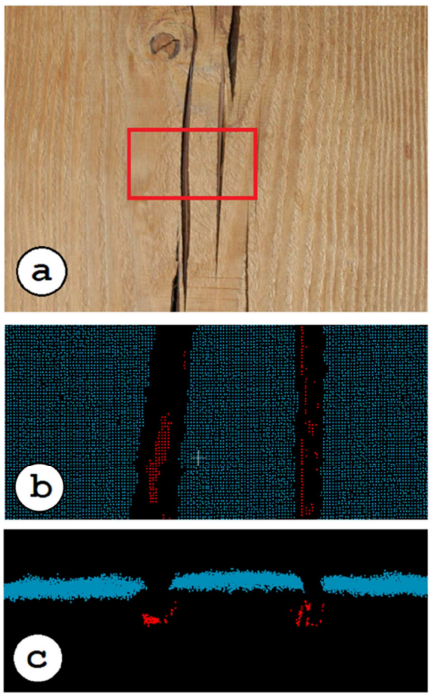

Figure 4. Example of points inside a crack that may remain after segmentation. a) Cracks in the beam. b) Plan view of the point cloud (red points are cleaned by fitting suitable polynomial surfaces) c) Profile view of the point cloud.

In order to remove these inside points, polynomial surfaces (*Pn*) are fitted to the segmented point cloud of the face *F(x,y,z)*. For this task, a plane is not sufficient because the surface of a timber beam is in general not fully flat. After surface adjustment, all points above a distance, *L*, from the surface *Pn* are removed (Figure 5d). *L* is a value that depends on the noise level of the laser scanner following Equation (1)

$$L = \sigma\ \alpha_c \qquad (1)$$

where σ is the nominal precision of the laser scanner and α_c an adjustable range for cleaning, obtained experimentally. This step results in a cleaned point cloud *F´(x,y,z).*

2 .2. 2D Projection and new 2D coordinate system

A plane is fitted to the cleaned point cloud $F'(x,y,z)$ of the face by orthogonal regression. All points are projected orthogonally on this plane, after a new coordinate system is fixed in the face (Figure 5e). The origin is always placed in the left bottom corner of the face. Subsequently all points are changed to the new coordinate system obtaining a new point cloud $N(x,y)$ in 2D.

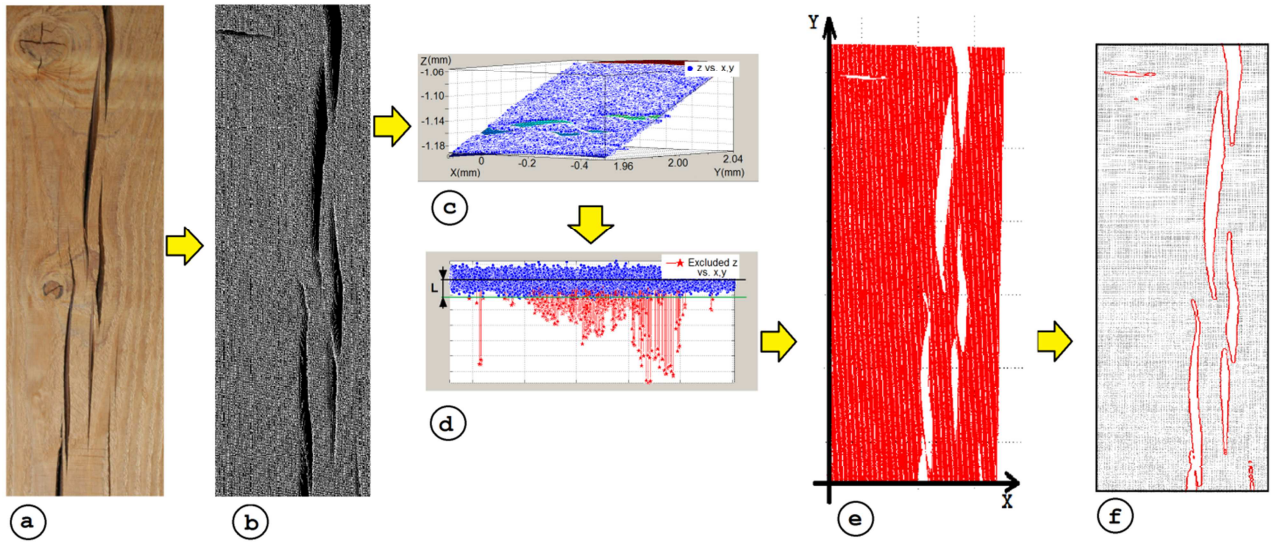

Figure 5. (a) Face of a timber structure with cracks. (b) Point cloud of the face timber structure. (c) Polynomial surfaces fitted to the segmented point cloud of the face. (d) Removed points located beyond a distance, L, from the polynomial surface. (e) Points projected on an orthogonally plane. (f) Cracks found after using Alpha-shapes.

2.3. Determining crack outlines

In this step Alpha-shapes are applied for detecting the outlines of cracks. Alpha-shapes [29] can be regarded as a family of "shapes" associated with a finite set of points. This approach generalizes the convex hull and allows finding non-convex shapes and holes in a finite set of points. The result of this method is the shape generated by consecutive point pairs that can be touched by an empty circle of diameter alpha (Figure 6). The obtained result depends directly on the choice of the diameter alpha (D_α). In 2D, Alpha-shapes have been used successfully for finding building roof edges in LiDAR data [30] and also, for estimating parametric plane models and determining boundaries of planar

patches in buildings in large-scale and noisy raw point clouds [31]. In both these works, Alpha-shapes are used for finding the outside edges of large surfaces. In our case however Alpha-shapes are applied for estimating the location of the inside edges of small holes in the wood, where the diameter D_α is critical in obtaining an optimal result.

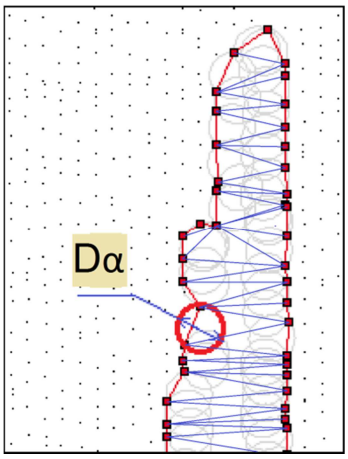

Figure 6. Alpha parameter D_α. The area of the crack is the sum of the area of all triangles.

For too small values, the results outline individual points while for too large values no crack is found at all. Because of this, it is necessary to identify that value D_α that enables finding all cracks with maximal accuracy. When Alpha-shapes are used, not only true cracks are detected, but also some false positives may be obtained (Figure 7).

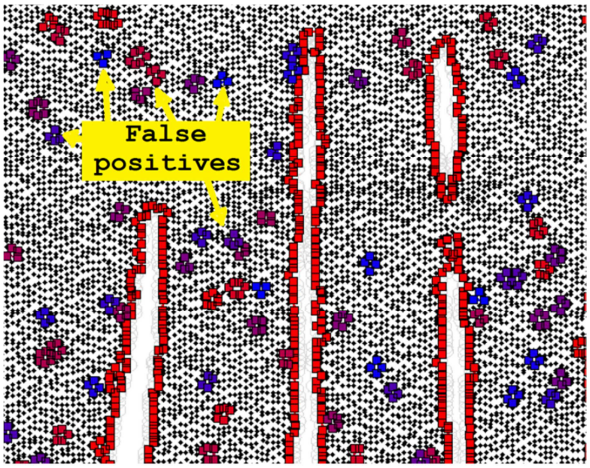

Figure 7. Example of false positives detected by Alpha-shapes.

It should be noted that if the value D_α is further reduced below a certain critical value, the number of obtained false positives increases exponentially. The reason for this behavior is that for too small D_α, natural gaps in the point cloud due to the limited point density are reported. Figure 8 shows from left to right the effect of decreasing the diameter D_α of the alpha circle.

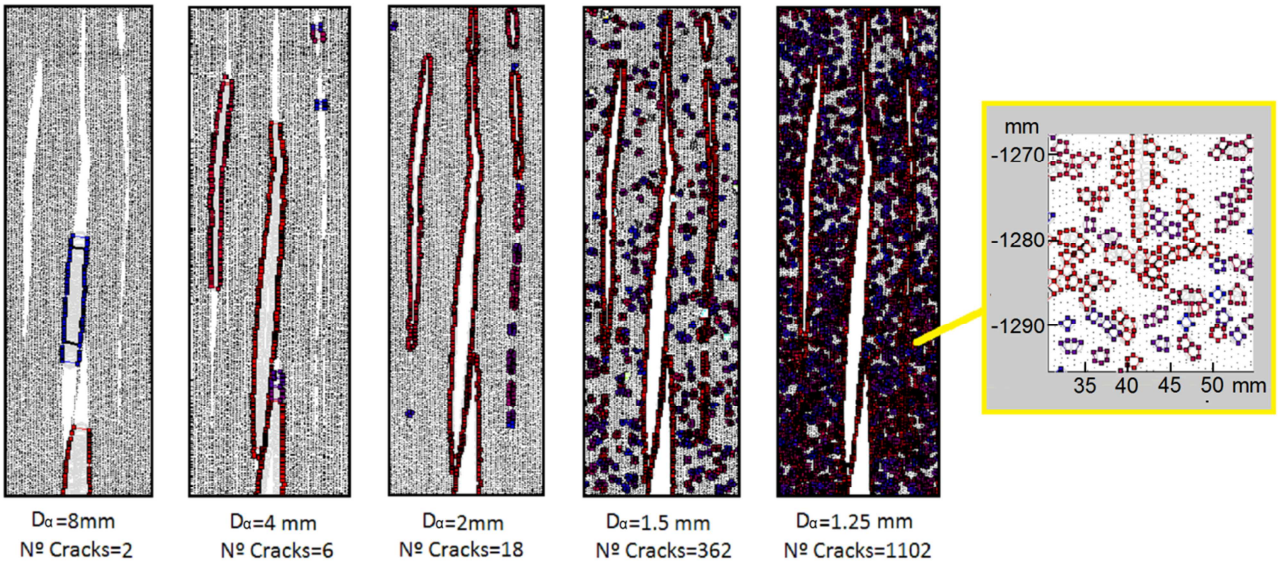

Figure 8. Number of possible cracks found according to the value of the diameter D_α.

In the proposed algorithm the Alpha-shape function starts by using a value D_1 for the diameter of the alpha circle. This value is directly proportional to the density of points on the face of the beam and is calculated according to Equation 2.

$$D_1 = 3\sqrt{\frac{W*H}{Np}} \qquad (2)$$

where W is the face width, H is the face length, N_p the number of points in the face and 3 a value obtained experimentally.

The number of cracks n_1 found when using value D_1 is calculated. Progressively, the value of D_α is decreased until a value D_m where the number of cracks found exceeds a value n_t (Equation 3).

$$\begin{cases} \text{While } n_i \leq n_t \quad i = 1, \dots, m \\ D_{i+1} \leftarrow (D_i - P) \\ n_{i+1} \leftarrow \alpha\_\text{shape}\big(N_p(x,y)\big)\ to\ D_{i+1} \\ else \\ found\ cracks \leftarrow \alpha\_\text{shape}\big(N_p(x,y)\big)\ to\ D_i \end{cases} \tag{3}$$

Here, n_i is the number of cracks found by the Alpha-shape; n_t is a threshold for the number of cracks, which is calculated based on the ratio n_i/N_p where n_i is the number of cracks found and N_p is the number of points on the beam face to be analyzed; D_i is the value of D_α used; P is the step value for decreasing D_i. For common point resolutions between 0.1 and 2mm as are expected from a phase-shift terrestrial laser scanner, a step value (P) for decreasing D_i equal to 0.25 mm is enough; Finally, $N_p(x,y)$ is the point cloud sampling the beam face in 2D projection.

2.4. Labeling each crack

As mentioned in the previous section, when Alpha-shapes are used, not only the cracks are detected, but also some false cracks (see Figure 7). To mitigate this problem, we need to differentiate between true and false cracks. For this task, first a minimum area A_{min} is fixed. The minimum area used should be greater than the area of the circle with diameter D_1. This parameter is adjustable by the user and depends on the minimum crack area the user wants to detect. In this paper the A_{min} used was 50 mm^2 .Subsequently the area of each detected crack is calculated. For this calculation, the algorithm triangulates the points that define the edge of the crack as estimated by the Alpha-shape (Figure 6). The area of the crack is the sum of the areas of all triangles. If this area is bigger than A_{min} this is a true crack and it is labeled, otherwise it is deleted (Equation 4).

$$\begin{cases} \text{if } A_i \geq A_{\min} \quad i = 1, \dots, n \\ Labeled: L_j \leftarrow \text{Crack } A_i \quad j = 1, \dots, k \\ \text{else} \quad\quad Deleted \leftarrow \text{Crack } A_i \end{cases} \tag{4}$$

Here A_i is the area of each candidate crack, n is the number of candidate cracks, A_{min} denotes the minimum area, L_j is the identification number of each true crack and k is the number of true found cracks.

2.5. Analysis of the geometric characteristics of each crack

Each crack is analyzed based on the points that define its edge. The results are calculated in the system coordinates fixed for the beam face. The data defined for each crack are:

i) Main direction. This is calculated by orthogonal regression from the point cloud of the crack (Figure 9).

ii) Area. Calculated in the previous step.

iii) Centroid of the crack. This is estimated from the centroids of each triangle contributing to the area of the crack (Equation 5-6). These triangles are obtained by a triangulation of the points that define the edge of the crack.

$$X_{ce} = \frac{\sum x_i A_i}{A_c} \quad i = 1, \dots, n \tag{5}$$

$$Y_{ce} = \frac{\sum y_i A_i}{A_c} \quad i = 1, \dots, n \tag{6}$$

Here X_{ce} and Y_{ce} are the coordinates of the centroid of the crack, x_i and y_i are the coordinates of the centroid of the each triangle, n is the number of triangles, A_i is the area of each triangle and A_c is the crack area. For estimating the centroid of the crack just taking the mean of the crack edge points is not suitable, because in many cases the number of points on one side is much higher than on the other.

iv) Length of the crack. Length calculated in the principal direction of the crack.

v) Maximum width. This parameter is calculated by measuring the maximum distance between crack edge points orthogonal to the main direction. For this purpose the crack width is calculated at constant intervals (in this paper at intervals of 10 mm because such interval provides sufficient resolution for typical cracks in timber beams) and the maximum width is reported.

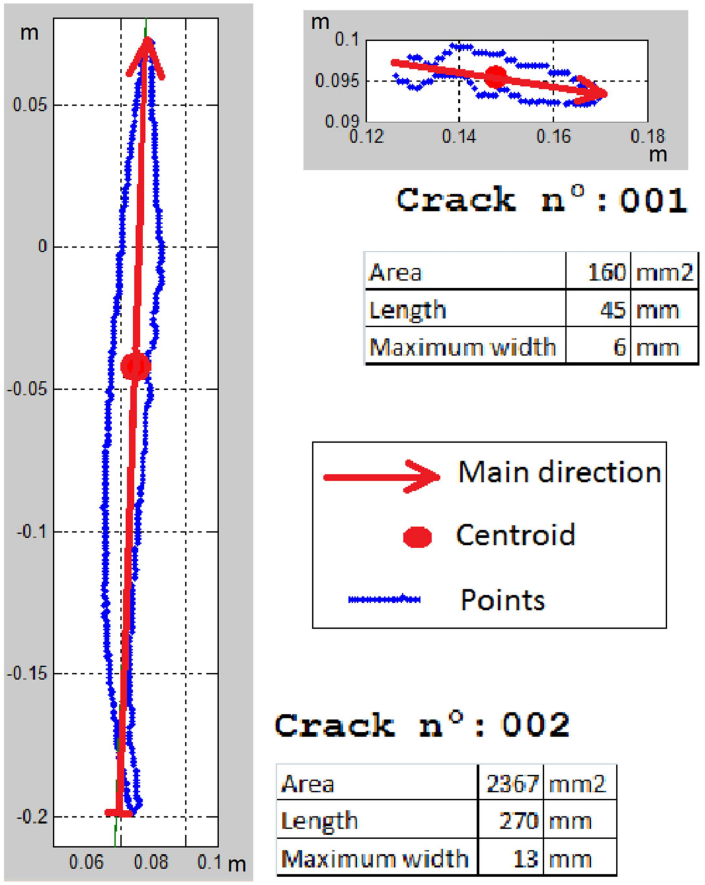

Figure 9. Example of two cracks with their geometric characteristics

Finally, a data file with all geometric characteristics of each found crack is obtained. In future work, the size, location and direction could be used to determine whether a crack is dangerous.

3. Test and results

In order to verify the correct operation of the developed algorithm, two types of tests were performed: first on laboratory specimens and, second, on a real timber structure . A phase-shift terrestrial laser scanner FARO Photon 120/20 is used to collect point clouds in these tests. This laser scanner measures distances over a range of 0.6 m to 120 m, with a ranging error of ±2 mm, at 25 m distance in normal illumination and reflectivity conditions. The beam diameter at exit equals 3.3 mm and the beam has circular shape. The field of view is 360º horizontal and 320º vertical. The acquisition rate varies from 122000 to 976000 points per second with a maximum angular resolution of 0.009º. The algorithm is implemented in MATLAB (MathWorks, Natick, Massachusetts, USA).

3.1 Laboratory test

Firstly several laboratory tests are performed for checking the correct operation of the algorithm developed for detecting the geometric characteristics of the cracks, as well as detecting its growth between epochs. For this purpose a polyurethane specimen of 500x210x90 mm^3 is used (Figure 10a). This material is chosen as it gives us an easy way to make cracks of a proper size and orientation. While in addition it allows us to perform a simulation of crack growth. A template drawn by computer is used to mark several cracks on the surface of the polyurethane specimen. Next the indicated cracks are cut by a cutter at a constant depth of 90 mm. Epoch 1 features four different cracks A, B, C, D (Figure 10b). In Epoch 2 (Figure 10c), crack A is kept the same, while crack B is increased to twice its original width and length, crack C is increased twice in length, crack D is increased twice in width and crack E is new. The laser scanning is performed at incidence angles of approximately 0º, 15º, 30º and 45º. The scanner center is positioned at the same elevation as the center of the specimens (see Figure 10d).

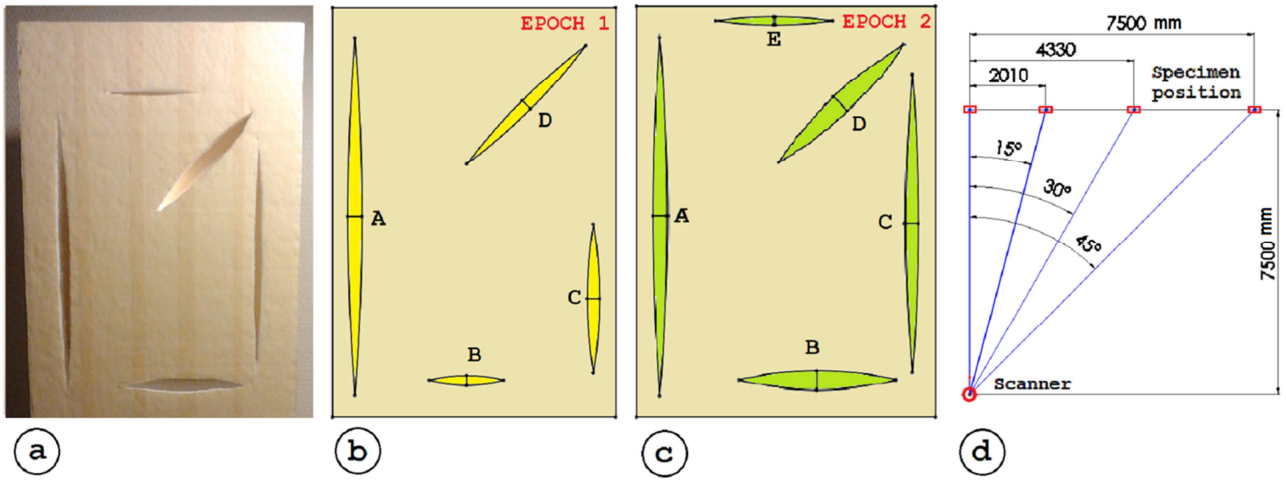

Figure 10. a) The specimen of Epoch 2. b) Drawing of the specimen for Epoch 1. c) Drawing of the specimen for Epoch 2. d) Plan of the laboratory test.

The developed algorithm was applied for analyzing the geometric characteristics of each crack for each position in both epochs. The obtained results are compared with validation measurements of the cracks and its direction. A caliper is used to obtain the validation measurements. Besides, the growth between Epoch 1 and Epoch 2 is analyzed. The average point resolution is between 1.4 mm and 2.1 mm, depending on the scanning angle. After segmenting the beam face, outliers are removed by evaluating the distance of individual points to a polynomial surface fitted to the beam face points, with a value of α_c equal to 2.0. The measurements of each crack obtained by the algorithm for different incidence angles in Epoch 2 are shown in Table 1. The detected minimum crack width directly corresponds to the value of the alpha diameter used (see Table 1). The differences in the width of each crack as estimated by the algorithm are 2 mm at incidence angles of 0 – 30º, and 4 mm at incidence angle of 45 º. In all cases, the crack width based on the scans was overestimated by on average 5 mm. The crack lengths were underestimated by maximally 10 mm for incidence angles between 0º and 15º, and by maximally 30 mm for incidence angles of 30º (real length is measures for a minimal width of 2 mm). For incidence angles of 45º inconsistent results are obtained.

		Real	Algorithm			
	Scan angle		0º	15º	30º	45º
	Average point resolution (mm)		1.4	1.5	1.6	2.1
	D alpha-shape (mm)		2.2	2.4	3.2	5.0
Crack A	Width (mm)	8	13	12	13	16
	Length(mm)	190	189	185	160	144
	Angle (º)	90	90	90	90	90
	Area (mm^2)	1500	1786	1609	1552	1484
Crack B	Width (mm)	11	16	17	17	17
	Length(mm)	90	86	89	90	90
	Angle (º)	0	0	0	1	1
	Area (mm^2)	875	1080	1120	1164	1219
Crack C	Width (mm)	6	12	10	12	13
	Length(mm)	155	154	145	126	86
	Angle (º)	90	90	90	90	90
	Area (mm^2)	990	1282	1063	1038	781
Crack D	Width (mm)	13	19	18	17	19
	Length(mm)	105	102	98	95	93
	Angle (º)	45	45	45	45	46
	Area (mm2)	1150	1455	1254	1167	1133
Crack E	Width (mm)	7	12	11	13	12
	Length(mm)	70	64	69	70	86
	Angle (º)	0	0	0	0	1
	Area (mm^2)	480	586	653	675	781

Table 1. Summary of the geometric characteristics of the cracks found by the algorithm for different incidence angles for Epoch 2.

The differences in the crack area as estimated by the algorithm for the different scan positions are all below 300 mm^2 at incidence angles between 0 and 30º. These values are all within 30 % of the crack area. The differences exceed 45% in some cases at an incidence angle of 45º. Difference in percent between the real value for each crack area and the area obtained by the algorithm for different incidence angles for Epoch 2 is shown in Figure 11.

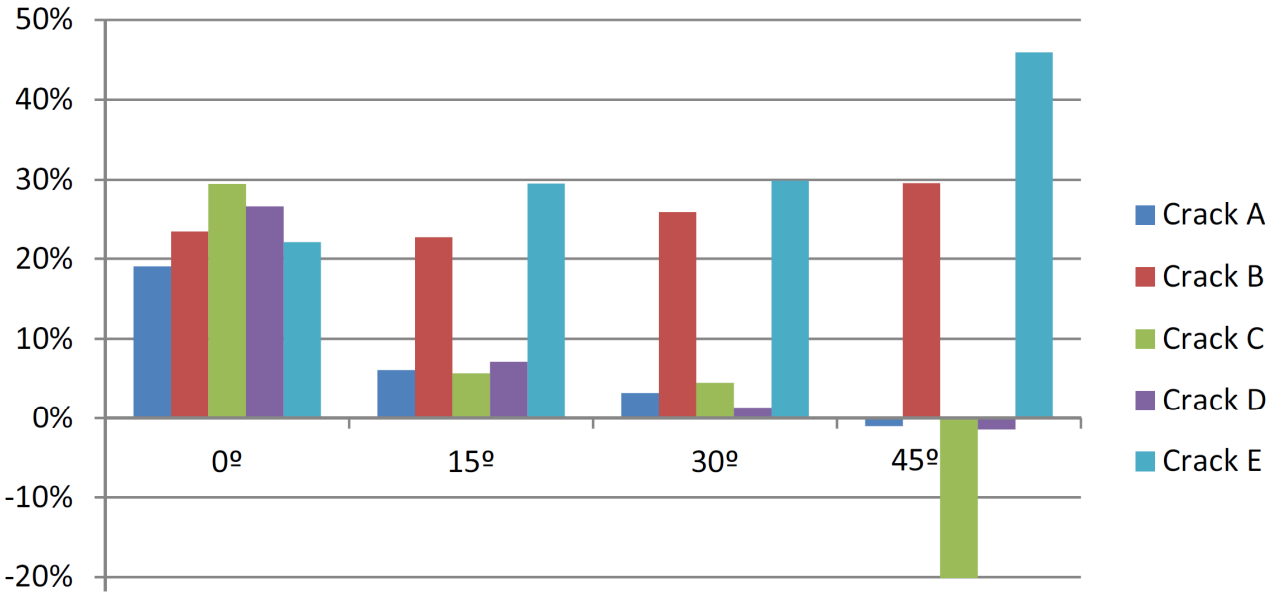

Figure 11. Difference in percent between the real value for each crack area and the area obtained by the algorithm for different incidence angles for Epoch 2.

The differences in the increase in area of each crack estimated by the algorithm between Epoch 1 and Epoch 2 for the different scan positions are all within 300 mm^2 at incidence angles of 0–30º. The growth found by the algorithm between Epoch 1 and Epoch 2 for different incidence angles is shown in Figure 12.

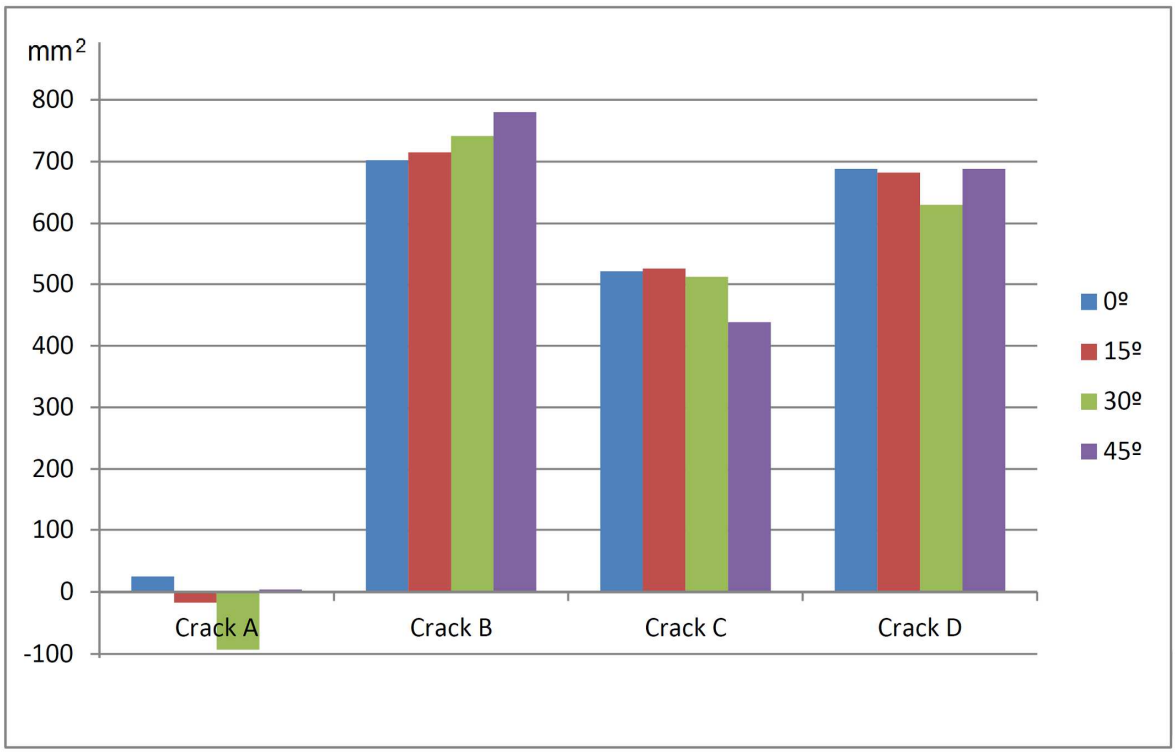

Figure 12. Growth found by the algorithm between Epoch 1 and Epoch 2 for different scan angles.

3.2 Real structure

The developed algorithm also has been tested on a real timber structure. This structure is situated in Zoetermeer (The Netherlands) and nowadays supports a restaurant (Figure 13). The main dimensions are 13 m wide, 21 m long and 10 m high. The building was built around 2009. Its structure has been made of solid timber beams (wood species: *Pinus sylvestris L.*) with cross section of 450 mm x 300 mm. The structure has a lot of cracks (Figure 13b).

Figure 13. a) Outside of the scanned real structure. b) Inside of the scanned real structure.

Inside the building, three different scans are performed from 3 different scanner positions. The laser scanning is performed at high resolution (976000 points/s). Six beams (column, diagonal brace and beam A and B) of the timber structure (Figure 13b) are analyzed by the algorithm. The average point resolution on these specimens is below 1 mm. The files obtained are stored for future comparison. After segmenting, and outlier removal cracks were detected using a value α_c equal to 2.5. A total of 54 cracks have been found by the algorithm in the 6 analyzed beams; 11 cracks turn out to be false. These false cracks are du e to regions occluded by wood pins, speakers and lamps over the beam face

(Figure 14). The algorithm is found suitable for cracks with a width of over 3 mm; 26 small cracks with widths equal or less than 3 mm are not detected by the algorithm. When two cracks are very close (separated by less than about 5 mm), the cracks are merged by the algorithm (Figure 14c).

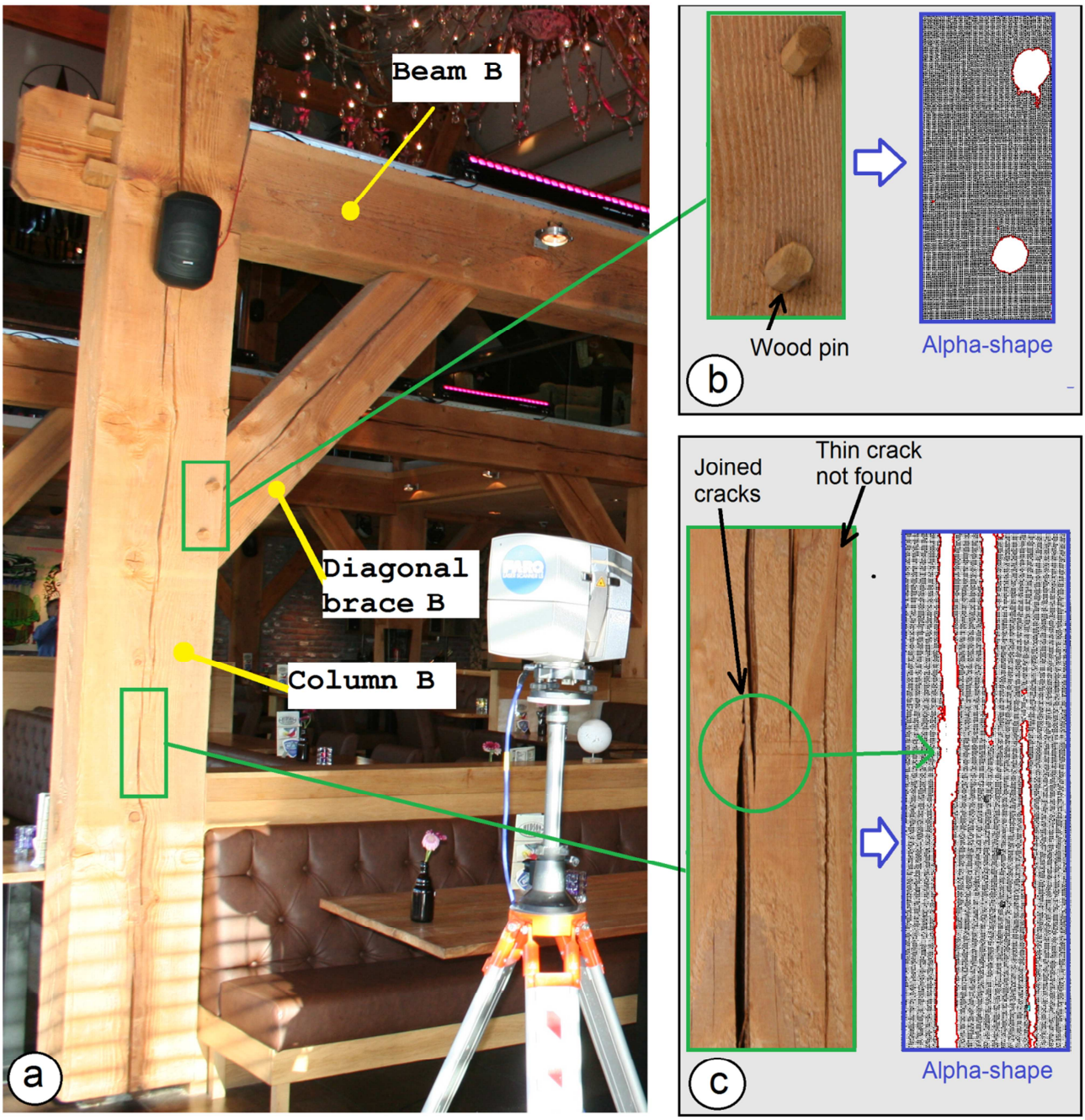

Figure 14. a) Column, diagonal brace and beam B analyzed by the algorithm. b) False cracks due to occluded regions by the wood pins. c) Two cracks joined by the algorithm and thin crack not found.

In all cases the maximum width is overestimated by 4 mm on average. The geometric characteristics of the cracks found in column A by the algorithm are shown in Table 2. The calculated length is until a minimum width equal to the used value of the diameter alpha. A summary of the results found for the six specimens of the timber structure analyzed by the algorithm are shown in Table 3.

Crack label	CI2-1	CI2-2	CI2-3	CI2-4	CI2-5	CI2-6	CI2-7	CI2-8	CI2-9	CI2-10	CI2-11	CI2-12	CI2-13	CI2-14	CI2-15	CI2-16	CI2-17	CI2-18	CI2-19
Area (mm2)	4227	1444	4819	8654	370	270	3207	2814	6419	1080	575	3581	8385	1095	892	248	333	377	351
Length (mm)	359	216	408	593	50	45	282	305	578	187	30	311	582	159	159	41	44	80	69
Maximun width (mm)	16	8	20	19	10	10	15	16	16	7	26	14	19	10	8	9	17	7	7
Mean width (mm)	12	7	12	15	7	6	11	9	11	6	19	12	14	7	6	6	8	6	6
Angle to main axi (º)	2	2	2	2	90	90	2	2	2	2	90	2	1	2	2	85	88	2	2

Table 2. Geometric characteristics of the cracks found in column A by the algorithm.

	Column A	Diag. Brace A	Beam A	Column B	Diag. Brace B	Beam B
Nº of cracks	19	4	1	13	4	2
Nº of cracks > 1000mm2	11	2	0	7	3	1
Mean area (mm2)	2584	1786	475	1744	2094	1025
Maximum area (mm2)	8654	9461	475	11039	8130	1756
Mean width (mm)	9	10	5	8	11	6
Maximum width (mm)	26	16	7	29	18	11
Mean length (mm)	236	180	95	219	182	176
Maximun length (mm)	593	595	95	806	662	289

Table 3. Summary of results found by the algorithm for six beams of the timber structure.

Besides cracks also knots were derived from point clouds of the 3D laser scan (Figure 15b). Even small cracks within the knots are recognized. An attempt has been made to determine the depth of the cracks before deleting the points inside the crack (Figure 15c). Because of the complex morphology of the cracks within the beam, the point clouds in general do not represent the true depth geometry. Only if the laser beams are directed perpendicular on the crack at which the crack has a one- dimensional depth, the model can reconstruct the depth.

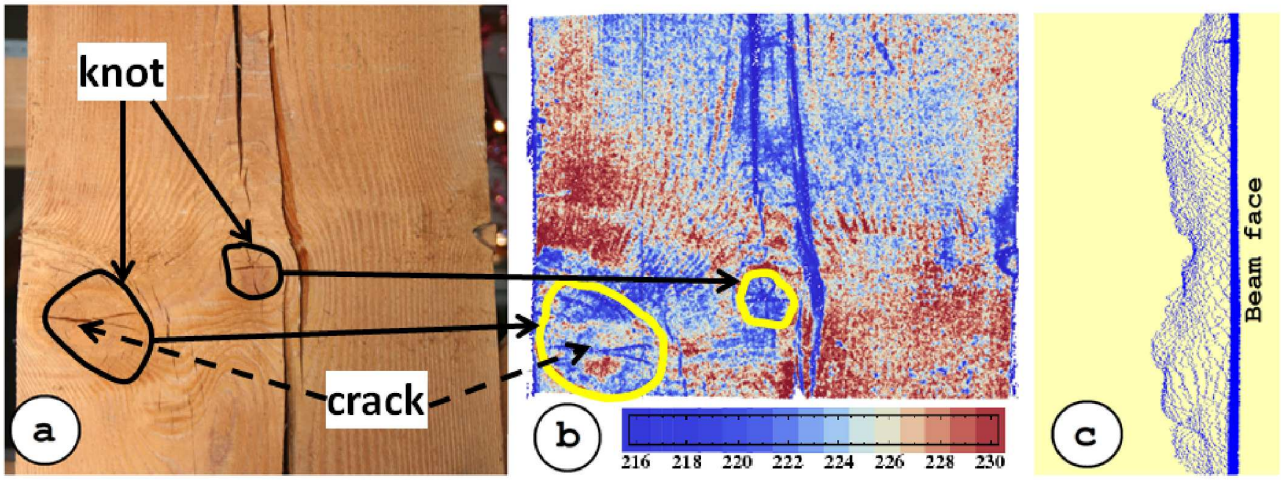

Figure 15. (a) Face of a beam with cracks. (b) Point cloud of the beam face. Points are colored by intensity as indicated by the color bar (c) Points inside a crack.

4. Discussion

The obtained results prove that the proposed algorithm is suitable for finding cracks automatically in timber beams, as well as detecting its growth between epochs. But the results also show that there are several issues.

-*Crack width.* All results have overestimated the maximum crack width (Table 1). This matches other experimental works performed by Laefer et al. [32] and Laefer et al. [24]. We have two possible explanations for this overestimation: point sampling and mixed pixels. Considering point sampling: our current approach estimates the width of a crack based on points classified as edge points by the Alpha-shapes method. These edge points are always situated on the beam face.

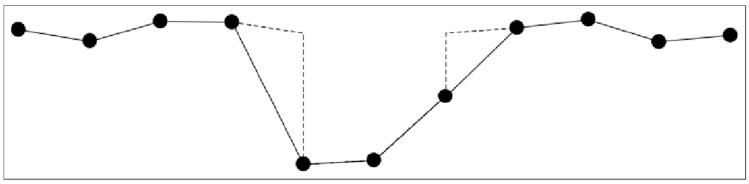

Figure 16. Profile of a synthetic crack.

Compare the synthetic situation in Figure 16. The three lower points in the middle are from the crack, the other point are on the beam face. In fact there are two extreme reconstructions of the surface along the profile in the figure. One is indicated by the connected line segments. In this case the crack starts, on both sides, directly at the two edge points. The other situation is indicated by the dashed line segments. In this case the beam face is continuing after the found edge points and the crack only starts at the location of the two extreme crack points. Given the discrete sampling of a laser scanner, it is not possible to indicate which reconstruction is better. The difference in the resulting crack width between the two reconstructions is about 2 *r,* with *r* the local resolution of the point cloud. On average we assume the crack starts on a distance 0.5 r from both edge points. This implies that, we could correct the width by applying Equation 7 in order to obtain a more realistic estimation of the crack width

$$Wc = W - r \qquad (7)$$

Here, *r* is the local resolution of the point cloud, *W* is the width as estimated by the methods described in Section 2.5, and *Wc* is the corrected width. Note that the point cloud resolution/point density is indeed varying throughout the point cloud as it depends on both range distance from scanner to surface, and local incidence angle. Therefore an implementation of this correction requires as additional input an estimation of the local point density, which can be obtained by counting the number of points sampling a beam part. Future work should address this improvement involving the use of Equation 7

Part of the overestimation is also expected to be a result of so-called mixed-pixels (edge loss), which occurs at spatial discontinuities [33] . The amount of overestimation depends notably on the diameter of the laser beam and on the scanning distance and on the angular resolution [33]. In this paper, the maximum width of the crack is overestimated by on average 4 mm at a distance of 2.5 m and by on average 5 mm at a distance of 7.5 m. Future work should address the automatic correction of this

overestimation as function of the beam diameter, scanning distance, incidence angle and resolution. Such correction should enable the correct estimation of the crack width.

The algorithm worked properly in finding cracks with a width larger than 3 mm in point clouds with average resolution below 1 mm from a point cloud sampling a real timber structure. According to the conclusions of the work by Laefer et al. [24] on crack detection limits, the minimum crack width found from LiDAR data mainly depends on the resolution of the point cloud, which depends on the technical specifications of the scanner (sampling step and beam width) the scan settings and the scan distance.

- *Crack length*. Overall the results tended to underestimate the length of the crack, this is because the crack length is only detected up to the width of the value of diameter alpha used, and the crack may continue at a lower width, but this is not detected. The crack length obtained for the same specimen in vertical cracks at different angles decreases significantly when the horizontal scan angle is increased. This is primarily due to the following factors: i) The increasing of the angle affects the quality of the point cloud [34], for larger incidence angles, lower point quality is obtained. ii) For larger angles the presence of mixed-pixels inside of the crack increases, especially in the more narrow zones of the crack which are very difficult to clean. iii) The resolution of the points decreases and therefore, it is necessary to use a higher width for the diameter alpha. However for horizontal cracks, the length does not decrease when the horizontal scan angle is increased because in these horizontal cracks the quality of the point cloud is not affected by different horizontal angles of scanning, as a consequence if the scan angle is increased also an increase in the calculated crack length can be estimated.

-*Crack area and growth.* The area obtained for each crack cannot be used directly because it is affected by the overestimation error of the maximum crack width, but this area value is useful to assess growth of cracks during different periods of time. Based on laboratory results it can be

determined that this new method can automatically detect crack area growth larger than 30 % (as minimum for distances of until 7.5 m and angles within 0-30 º) (Figure 12). Reported growths below 30% detected by the algorithm can also be due to errors in the point cloud and the algorithm and may not represent real crack growth. For angles of 45 ° the error increases significantly. Although the calculated area is always on the safe side (Figure 11), the error introduced by the measurement at the edges should be corrected for obtaining the correct area. As discussed in previous sections, future work should focus on correcting this problem automatically.

-*Survey area.* With a laser scanner with technical characteristics as used is this work, this algorithm works properly until a maximum incidence angle of 30 ° and until a distance of 7.5 m (point resolutions about 1.5 mm). For incidence angles of 45 ° the results are not correct. Therefore, survey areas of 7.5 x7.5 m^2 could be analyzed by a scanner positioned at of 7.5 m from the survey area. This is a suitable survey area and a suitable distance for many historical timber structures. In any case, for obtaining similar results, the distance from the laser scanner may be increased if a laser scanner with a higher sampling step and higher measurement accuracy is used. Obviously, it is possible to use this algorithm at larger distances with the same scanner but then the minimum crack width that is possible to detect is increased and the accuracy of the results decreases. Unlike for the laboratory tests, in the timber structure a larger value of α_c (2.5) was necessary for obtaining a correct segmentation. This is due to the fact that the surface of the timber beams was not fully flat, an important factor to consider when this method is applied on timber structures or other kinds of structures with similar surfaces.

It is noteworthy that the methodology and algorithm proposed in this paper are not only suitable for timber structures, but could also be used for other kinds of structures with cracks of similar characteristics.

5. Conclusions and future work

This paper proposes a new approach for the automatic detection of cracks in timber beams from LiDAR data as well as for controlling the growth of cracks during different periods of time. The obtained results prove that the proposed algorithm using Alpha-shapes is suitable for these tasks.

However, all results have overestimated the maximum crack width and therefore overestimated the crack area. Future work should address the automatic correction of the area and width overestimation as function of the beam diameter, scanning distance, incidence angle and resolution.

With a phase-shift terrestrial laser scanner with a ranging error of ±2 mm, a beam diameter at exit of 3.3 mm and a maximum angular resolution of 0.009º, the novel algorithm works properly for survey areas of 7.5 x7.5 m^2 scanned at distance of 7.5 m. Although these values are suitable for many historic wooden structures, future work should consider the use of other types of laser scanner and scanning greater distances. The methodology and algorithm proposed in this paper could also be used for other kinds of structures in case of cracks of similar characteristics.

According to the data file containing the size, location and direction of each identified crack, future work could determine if a crack is dangerous or not.

Advances in structural health controlling from LiDAR data have been achieved in recent years, however, no important progress has been made in the automatic search of cracks in structures, and therefore, this work represents an important advance in this direction.

Acknowledgments. This work has been partially supported by the University of Vigo through the " Axudas a estadias en centros de investigacion 2014" . Authors also want to give thanks to the Xunta de Galicia (Grant No: IPP055-EXP44 and EM2013/005; CN2012/269) and Spanish Government (Grant No:TIN2013-46801-C4-4-R; ENE2013-48015-C3-1-R; SICEMAM IPT-2012-363 1121-370000).

References

[1] Frech P. Beurteilungskriterien fuer Rissbildungen bei Bauholz im konstruktiven Holzbau. Bauen mit Holz 1987; 89(9):582-585 (in German).

[2] Van de Kuilen JWG, Gard W. Damage Assessment and Residual Service Life Estimation of Cracked Timber Beams. Advanced Materials Research 2013; 778:402-409.

[3] Hasníková H, Kuklík P. Various non-destructive methods for investigation of timber members from a historical structure. Wood research 2014; 59(3):411-420.

[4] Jasieńko J, Nowak T, Hamrol K. Selected methods of diagnosis of historic timber structures–principles and possibilities of assessment. Advanced Materials Research 2013; 778:225-232.

[5] Lechner T, Nowak T, Kliger R. In situ assessment of the timber floor structure of the Skansen Lejonet fortification, Sweden. Construction and Building Materials 2014; 58:85-93.

[6] Colla C. GPR of a timber structural element. In Ground Penetrating Radar (GPR), 13th International Conference on IEEE 2010; pp. 1-5.

[7] Barazzetti L, Scaioni M. Crack measurement: Development, testing and applications of an automatic image-based algorithm. ISPRS Journal of Photogrammetry and Remote Sensing 2009; 64 (3): 285-296.

[8] Sohn HG, Lim YM, Yun KH, Kim GH. Monitoring crack changes in concrete structures. Computer-Aided Civil and Infrastructure Engineering 2005; 20(1):52-61.

[9] Patricio MA, Maravall D. A novel generalization of the gray-scale histogram and its application to the automated visual measurement and inspection of wooden Pallets. Image and vision computing 2007; 25(6):805-816.

[10] Lee HM, Park HS. Gage-Free Stress Estimation of a Beam-like Structure Based on Terrestrial Laser Scanning. Computer-Aided Civil and Infrastructure Engineering 2011; 26(8):647–658.

[11] Liu W, Chen S. Hauser E. LIDAR based bridge structure defect detection. Experimental Techniques 2011; 35(6): 27-34.

[12] Olsen MJ, Kuester F, Chang BJ, Hutchinson TC. Terrestrial laser scanning-based structural damage assessment. Journal of Computing in Civil Engineering 2010; 24(3):264-272.

[13] Bosché F. Automated recognition of 3D CAD model objects in laser scans and calculation of as-built dimensions for dimensional compliance control in construction. Advanced Engineering Informatics 2010; 24(1):107–118.

[14] Zhang C, Arditi D. Automated progress control using laser scanning technology. Automation in Construction 2013; 36:108-116.

[15] Camarda M, Guarnieri A, Milan N, Vettore A. Health Monitoring of Complex Structure Using TLS and Photogrammetry. International Archives of the Photogrammetry, Remote Sensing and Spatial Information Sciences 2010; 38(Part 5):125-130.

[16] Riveiro B, Morer P, Arias P, De Arteaga I. Terrestrial laser scanning and limit analysis of masonry arch bridges. Construction and building materials 2011; 25(4):1726-1735.

[17] Cabaleiro M, Riveiro B, Arias P, Caamaño JC, Vilán JA. Automatic 3D modelling of metal frame connections from LIDAR data for structural engineering purposes. ISPRS Journal of Photogrammetry and Remote Sensing 2014; 96:47–56.

[18] Truong-Hong L, Laefer DF, Hinks T, Carr H. Combining an angle criterion with voxelization and the flying voxel method in reconstructing building models from LiDAR data. Computer-Aided Civil and Infrastructure Engineering 2013; 28(2):112–129.

[19] Walsh SB, Borello DJ, Guldur B, Hajjar JF. Data processing of point clouds for object detection for structural engineering applications. Computer-Aided Civil and Infrastructure Engineering 2013; 28 (7):495–508.

[20] Alessandri C, Mallardo V. Structural assessments of the Church of the Nativity in Bethlehem. Journal of Cultural Heritage 2012; 13(4):e61-e69.

[21] Balletti C, Berto M, Gottardi C, Guerra F. Ancient Structures and New Technologies: Survey and Digital Representation of the Wooden Dome of SS. Giovanni E Paolo in Venice. ISPRS Annals of Photogrammetry, Remote Sensing and Spatial Information Sciences 2013; 1(1):25-30.

[22] Oreni D, Brumana R, Cuca B, Georgopoulos A. HBIM for conservation and management of built heritage: Towards a library of vaults and wooden bean floors. ISPRS Annals of the Photogrammetry, Remote Sensing and Spatial Information Sciences 2013; 164:1-6.

[23] Van Goethem GRM, Van de Kuilen JWG, Gard WF, Ursem WNJ. Quality assessment of standing trees using 3D laserscanning. Proceedings COST E53: End user's needs for wood material and products. Delft, The Netherlands, 29-30 October 2008; pp.145-156.

[24] Laefer DF, Truong-Hong L, Carr H, Singh M. Crack detection limits in unit based masonry with terrestrial laser scanning. NDT & E International 2014; 62:66-76.

[25] Laefer DF, Gannon J, Deely E. Reliability of crack detection methods for baseline condition assessments. Journal of Infrastructure Systems 2010; 16(2):129-137.

[26] Huang J, Liu W, Sun X. A Pavement Crack Detection Method Combining 2D with 3D Information Based on Dempster-Shafer Theory. Computer-Aided Civil and Infrastructure Engineering 2014; 29(4):299-313.

[26] Sánchez-Aparicio LJ, Riveiro B, Gonzalez-Aguilera D, Ramos LF. The combination of geomatic approaches and operational modal analysis to improve calibration of finite element models: a case of study in Saint Torcato church (Guimarães, Portugal). Construction and Building Materials 2014; 70:118-129.

[27] Fischler MA, Bolles RC. Random sample consensus: a paradigm for model fitting with applications to image analysis and automated cartography. Communications of the ACM 1981; 24 (6):381-395.

[28] Schnabel R, Wahl R, Klein R. Efficient RANSAC for Point-Cloud Shape Detection. In Computer graphics forum, Blackwell Publishing Ltd 2007; 26(2):214-226.

[29] Edelsbrunner H, Mücke EP. Three-dimensional Alpha Shapes. ACM Transactions on Graphics (TOG) 1994; 13(1):43-72.

[30] Dorninger P, Pfeifer N. A comprehensive automated 3D approach for building extraction, reconstruction, and regularization from airborne laser scanning point clouds. Sensors 2008; 8(11):7323-7343.

[31] Zhang G, Vela PA, Karasev P, Brilakis I. A Sparsity-Inducing Optimization-Based Algorithm for Planar Patches Extraction from Noisy Point-Cloud Data. Computer-Aided Civil and Infrastructure Engineering 2015; 30:85–102.

[32] Laefer DF, Fitzgerald M, Maloney EM, Coyne D, Lennon D, Morrish SW. Lateral image degradation in terrestrial laser scanning. Structural Engineering International 2009; 19(2):184-189.

[33] Tang P, Akinci B, Huber D. Quantification of edge loss of laser scanned data at spatial discontinuities. Automation in Construction 2009; 18(8):1070-1083.

[34] Soudarissanane S, Lindenbergh R, Menenti M, Teunissen P. Scanning geometry: Influencing factor on the quality of terrestrial laser scanning points. ISPRS Journal of Photogrammetry and Remote Sensing 2011; 66(4):389-399.